 SDHM, vol.7, no.1, pp.65-81, 2011

An Application of Support Vector Regression for Impact Load Estimation Using Fiber Bragg Grating Sensors

Clyde K Coelho, Cristobal Hiche and Aditi Chattopadhyay

Abstract: Low velocity impacts on composite plates often create subsurface damage that is difficult to diagnose. Fiber Bragg grating (FBG) sensors can be used to detect subsurface damage in composite laminates due to low velocity impact. This paper focuses on the prediction of impact loading in composite structures as a function of time using a support vector regression approach. A time delay embedding feature extraction scheme is used since it can characterize the dynamics of the impact using the sensor signals. The novelty of this approach is that it can be applied on complex geometries and does not require a dense array of sensors to reconstruct the load profile at the point of impact. The efficacy of the algorithm has been demonstrated through simulation results on composite plates and wing structures. Trained using impact data at four locations with three different energies, the constructed framework is able to predict the force-time history at an unknown impact location to within 12 percent for a composite plate and to within 10 percent for a composite wing when the impact was within the sensor network region. Experimental validation is also presented on carbon fiber reinforced polymer wings showing low prediction errors even with small training sets.

Keywords: Damage estimation, support vector regression, time delay embedding, structural health monitoring, fiber Bragg grating sensors, impact, carbon fiber composite, wing.

1 Introduction

In the aerospace industry, there is a push towards condition based maintenance (CBM), as opposed to schedule based maintenance as the new maintenance paradigm. For aerospace vehicles that operate in complex, nondeterministic environments, the task of CBM which involves damage detection, identification, and useful life estimation becomes especially difficult. Additional complexities arise when composite structural components are involved. Survivability of composite structures subjected to dynamic contact loads is of critical importance in many aerospace ap-

plications. Low velocity impacts, can result in subsurface delamination that cannot be detected using visual surface inspection, even though they result in stiffness degradation and a significant loss in structural integrity, especially in thick composites. Impact damage is also highly dependent on the mass, shape, and velocity of the impacting objects. Currently, detection of this type of damage requires specialized non destructive evaluation (NDE) equipment like acoustic emission(Yu, Choi, Kweon and Kim(2006)), thermography (Genest, Martinez, Mrad, Renaud and Fahr(2008)), eddy current method (Şimşir and Ankara(2007)), and ultrasonic scanning (Aymerich and Meili(2000)). While use of certain NDE techniques can provide accurate estimates of damage, they all require that the structure being inspected be taken out of service and in some cases disassembled for inspection. For CBM to be viable, a structural health management (SHM) approach must be employed. A robust SHM framework requires the installation of a distributed sensor network so that damage measurements can be made quickly and frequently without significant effort or expense. Several types of sensor networks are being investigated, including strain gauges (Chan, Li and Ko(2001)), piezo transducers (Coelho, Das, Chattopadhyay, Papandreou-Suppappola and Peralta(2007)), and fiber optic sensors (Hiche, Liu, Seaver, Wei and Chattopadhyay(2009)). In this work, fiber Bragg grating (FBG) sensors have been chosen because they can be tailored to include multiple sensors on a single fiber resulting in a significant weight advantage when implemented on a large structure. Also, FBG sensors are low weight, require minimal space, and are immune to electromagnetic interference, which is a concern in the harsh operating environments of aerospace structures. However, FBGs only measure strain along the length of the fiber, a prediction scheme that can estimate loading using randomly oriented and dispersed sensors is key to damage state awareness since it could reduce installation time and the total number of sensors required to interrogate a complex structure. Unexpected impact loading on an aerospace structure can often lead to catastrophic failure. A passive detection approach (Grondel, Assaad, Delebarre and Moulin (2004)) is required since the structure can be constantly monitored and the operator can be notified immediately if there is an adverse event. A framework that can detect the location and estimate the strains induced at the point of impact will allow users to conduct detailed structural analysis and decide whether to take immediate action or schedule maintenance at a later date. The work in this paper focuses on estimating the load generated in a structure during an impact.

Although several approaches exist to determine the location of an impact, only a few also provide force-time history reconstruction of the impact event. One method to localize damage uses the guided waves that are emitted from the source of the impact. This method requires explicit knowledge of wave speed, which works rel-

atively well for homogenous structures (Betz, Thursby, Culshaw and Staszewski (2007)). In composites however, the wave propagation speed varies as a function of direction (Kundu, Das, Martin and Jata(2008)), which makes localization more difficult and this approach cannot be used to estimate the induced strains. Kim and Lee(2008), Lee(2008) used a Green's function approach to localize damage in an aluminum plate and reconstruct the load history. This approach assumes an infinite plate when solving for the transfer function between the impact location and sensor response. This same transfer function is used for the recovery of impact load which means it may not be applicable to small and/or complex structures. Park and Chang(2005) proposed a system identification technique that is based on training data from an experiment. Since the designed transfer function does not require a physical model, it represents the observed system response more accurately. However, the structural deformation must be linearly elastic during the impact process and the deformation of the structure must be small enough to neglect geometric nonlinearity. The approach used in this paper uses a machine learning technique to take data from experimental or modeling data and use it to build a model that can reconstruct the load history as a function of time. The support vector regression (SVR) technique, based on the popular support vector machines classifier (Coelho, Das and Chattopadhyay(2009)), and applied in other fields for time series prediction (Huang, Chen, Hsu, Chen and Wu(2004, Shin, Lee and Kim(2005)) was chosen because it performs well with high dimensional data sets and does not require extremely large training sets for generalization. Using the FBG sensor signals from finite element simulations and a time delay approach, impact force-time curves at the point of impact were estimated. The objective of this work is to build a data driven framework that can estimate the impact load at random locations accurately even in the absence of complete strain information. The approach developed in this paper has been tested using virtual sensing data from impact simulations on a composite plate and wing. Experimental validation was also conducted on a carbon fiber composite wing with surface mounted FBG sensors.

This paper is organized as follows. Sections 2 and 3 present a theoretical background on the method used for feature extraction and damage estimation respectively. The simulation setup and some details regarding data collection have been discussed in section 4. Section 5 demonstrates the effectiveness of the regression scheme through some selected results from simulated composite laminate and wing impacts and experimental validation. Section 6 presents some observations made from the present study along with suggestions for further improvement of the current work.

2 Time Delay Embedding

The sensor response collected from an FBG is a time series signal which can be defined as a sequence of measurements $x(t)$, at different instants of time, of an observable x acquired at regular time intervals. In time series applications, the dynamical information of the system can be extracted for a data set of scalar observations where each of these observations correspond to the projection of the systems' state vector in one dimension. Taken's theorem (Takens(1980)) states that it is possible to reconstruct the attractor in the phase space given $x(t)$. This can be achieved using the time embedding approach where a one-to-one differential mapping between a finite windowed time series can be constructed. Given a time series $x(t)$ with N number of data points, the state space vectors can be represented as follows,

$$y(t) = \begin{bmatrix} x(t) \\ x(t+\tau) \\ x(t+2\tau) \\ . \\ . \\ . \\ x(t+(D_E-1)\tau) \end{bmatrix} \tag{1}$$

where the time instant $t = nT_s$, T_s being the sampling time. Here D_E is the embedding dimension andτ is the time delay. The delay reconstruction makes it possible to view the dynamics in terms of a scalar field and hence the best surface fitting these points would represent the approximate dynamics of the system.

The time embedding approach is a very popular technique in the field of nonlinear dynamics and is commonly used to predict the future dynamics of a system. To ensure proper reconstruction, the embedding dimension and the time delay have to be assigned properly. In data driven approaches, while introducing delay in experimental data sets, the choice of the time delay is considered to be a very important step. This is because when τ is chosen to be very small compared to the internal time scale of the system, the successive components of the delay vectors $x(t)$ and $x(t+\tau)$ are almost linearly dependent, that is, they are highly correlated. On the other hand, a very large delay τ, can result in an "over-folding" of the attractor. The value of D_E and τ chosen for the experimental results presented here are 5 and 2.56 x 10^{-4}s respectively. The values were chosen arbitrarily based on user experience and 5 fold cross validation on the training set was used to make sure these values were appropriate.

3 Support Vector Regression

Support vector machines(SVMs) (Vapnik and Sterin(1977)), a popular machine learning based approach, has been adapted for regression (Smola(1996)) problems by using an alternative loss function. The basic idea behind support vector regression is the construction of a regression line $f(\vec{x})$ that has less than an ε deviation from the target responses y for a majority of the training data and is, at the same time, as smooth as possible. Smoothness here refers to the complexity of the constructed model. If $f(\vec{x})$ is smooth or "flat", it will be better at rejecting noise but worse at fitting non smooth training data when compared with non-smooth $f(\vec{x})$. This tradeoff is controlled by appropriately tuning the hyperparameters during optimization.

Consider a data set S that will be used to build a support vector regression model. S is given by,

$$S = \{(\vec{x}_i, y_i)\}_{i=1}^{m}, \quad \vec{x} \in \mathrm{R}^n,\ y \in \mathrm{R} \tag{2}$$

where $\vec{x}$ is a feature vector, y is a target function value and, m is the total number of training points. If this data cannot be linearly regressed as is the case with a lot of real world data, a nonlinear regression approach is required. To solve this problem, consider the following linear estimation function (Lu, Lee and Chiu(2009)) (Figure 1),

$$f(\vec{x}) = \vec{w} \cdot \Phi(\vec{x}) + b \tag{3}$$

where $\Phi(\vec{x})$ denotes a mapping function from the input space to a high dimensional feature space where the inputs can be linearly correlated with the system outputs, $\vec{w}$ is a weight vector, and b is a constant offset term.

There are a number of loss functions that can be used in the SVR formulation. Although quadratic, Laplace and Huber's loss function are common, they do not allow for the selection of a sparse set of support vectors. For this reason, an ε-insensitive loss function (Figure 1) which does not penalize data points within an ε-radius tube around the regression function is used. A point which deviates from the regression function by an amount larger than ε, gets penalized by an amount proportional to its distance from the exterior of the ε-insensitive zone (Figure 1). These deviations on either side of the zero penalty zone are measured using the slack variables ξ and ξ^*. The loss function is given by,

$$L_\varepsilon(f(\vec{x}), y) = \begin{cases} |f(\vec{x}) - y| - \varepsilon & if\ |f(\vec{x}) - y| \geq \varepsilon \\ 0 & otherwise \end{cases} \tag{4}$$

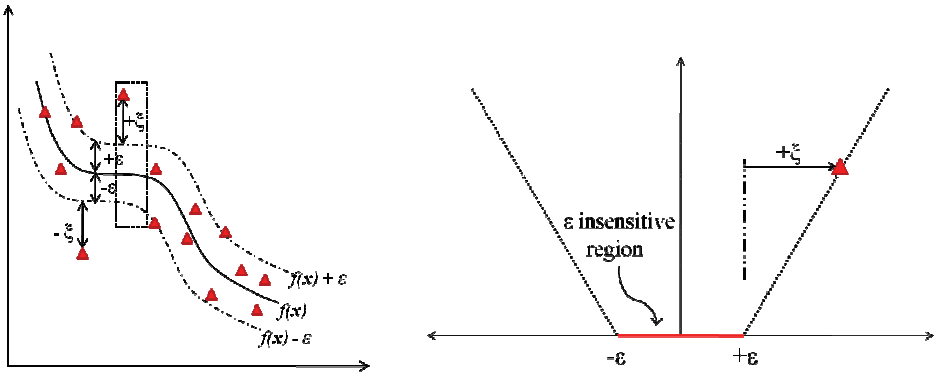

(a) (b)

Figure 1: Schematic of (a) SVR construction and, (b) ε insensitive tube

The variables $\vec{w}$ and b from Eqn (3) can be estimated by minimizing the risk function given by,

$$R(C) = C\frac{1}{n}\sum_{i=1}^{n} L_\varepsilon\left(f\left(\vec{x}_i\right), y_i\right) + \frac{1}{2}\left|\vec{w}\right|^2 \tag{5}$$

where $\frac{1}{2}\left|\vec{w}\right|^2$ is the regularization term used to find the flattest function with sufficient approximation qualities and C is a user defined constant controlling the trade-off between the empirical risk (training error) and the regularization term which penalizes complexity.

The risk function in Eqn (5) can be transformed into a constrained optimization problem using the slack variables as shown.

$$\underset{w,b,\xi,\xi^*}{Min}\ R_{reg}(f) = \frac{1}{2}\left|\vec{w}\right|^2 \tag{6}$$

$$\text{subject to, } \begin{cases} y_i - (\vec{w}\cdot\Phi(\vec{x}_i)) - b \le \varepsilon + \xi_i \\ (\vec{w}\cdot\Phi(\vec{x}_i)) + b - y_i \le \varepsilon + \xi_i^* \\ \xi_i^*,\ \xi_i \ge 0,\ \text{for } i = 1,,n \end{cases} .$$

Equation (6) can be converted into its dual Lagrangian form with the Karush-Kuhn-

Tucker (KKT) conditions of optimality to yield,

$$L_d(\alpha,\alpha^*) = -\varepsilon\sum_{i=1}^{n}(\alpha_i^*+\alpha_i)+\sum_{i=1}^{n}(\alpha_i^*-\alpha_i)y_i - \frac{1}{2}\sum_{i,j=1}^{n}(\alpha_i^*-\alpha_i)\left(\alpha_j^*-\alpha_j\right)K(\vec{x}_i,\vec{x}_j) \quad (7)$$

$$\text{subject to, } \begin{cases}\sum_{i=1}^{n}(\alpha_i^*-\alpha_i)=0\\ 0\le\alpha_i^*,\ \alpha_i\le C,\ i=1,,n\end{cases}.$$

The KKT conditions satisfied by the solution are $\alpha_i\alpha_i^*=0$. Solving the Lagrangian optimization problem, the general form of the SVR based regression function is given by,

$$f(\vec{x}) = \sum_{i=1}^{n}(\alpha_i-\alpha_i^*)K(\vec{x},\vec{x}_i)+b^*. \quad (8)$$

where the optimal weight vector and bias of the regression hyperplane are given by,

$$\begin{aligned}\vec{w}^* &= \sum_{i=1}^{n}(\alpha_i-\alpha_i^*)K(\vec{x},\vec{x}_i)\\ b^* &= -\frac{1}{2}\sum_{i=1}^{n}(\alpha_i-\alpha_i^*)\left(K(\vec{x}_i,\vec{x}_p)+K(\vec{x}_i,\vec{x}_q)\right)\end{aligned} \quad (9)$$

In this work, the mapping of the data from the input space to a high dimensional feature space was carried out using a Radial Basis Function (RBF) kernel (Coelho, Das and Chattopadhyay(2009)) defined as,

$$K(\vec{x},\vec{x}_i) = e^{-\frac{\|\vec{x}-\vec{x}_i\|}{2\sigma^2}} \quad (10)$$

4 Finite Element Model

4.1 Composite Plate Model

A finite element model simulating impact on a twill weave composite plate has been developed using ABAQUS Explicit. The dimensions of the plate specimen are 12in x 12in x 0.06in and the material properties of the twill weave composite ply is presented in Table 1. A total of 15 simulations have been conducted, representing impacts at five different locations (Figure 2(a)), (3,9), (4,4), (6,5), (8,3), (10,10), each with impact energies of 0.5J, 12.5J and 50J. The bulk elastic

properties along with the failure strength of the woven graphite epoxy plies were calculated at the microscale using a micromechanics analysis, MAC/GMC, which is based on the Generalized Method of Cells approach(Bednarcyk and M.(2002)). The four ply laminate was modeled using continuum shell elements with clamped boundary conditions. A hemispherical impactor head (Figure 2(b)) with a 1.4in diameter was used. Hard contact and frictionless impact conditions were applied to model the interaction between the tup and the composite structure. The virtual FBG sensor data, from where the strains measurements were obtained, are presented in Table 2.

Table 1: Material properties for twill weave composite.

E_{11} (GPa)	78.5600
E_{22} (GPa)	78.5600
E_{33} (GPa)	9.8330
ν_{12}	0.0252
ν_{13}	0.0392
ν_{23}	0.0392
G_{12} (GPa)	5.4170
G_{13} (GPa)	3.7860
G_{23} (GPa)	3.7860

Table 2: FBG sensor locations on the composite plate

Sensor Number	x-coordinate (in)	y-coordinate (in)	Measured strain component
S1	3.875	2.750	ε_{yy}
S2	8.125	2.750	ε_{yy}
S3	9.375	6.750	ε_{xx}
S4	6.000	9.250	ε_{yy}
S5	2.625	6.750	ε_{xx}

4.2 Composite Wing Model

A four ply twill weave composite wing has also been simulated using ABAQUS Explicit. The cross section of the wing is based on the NACA 0012 airfoil. The simulated wing has an 11in chord length and a 17in span, with simply supported edges (Figure 3(a)). A total of 15 simulations have been run consisting of impacts at 5 locations [(2,6), (5,8), (8,4), (6.5,5), (13,3)] (Figure 3(a)). The impact energies

simulated at each location were 5J, 15J and 50J. The material properties used in the simulation were calculated using the MAC/GMC code. Continuum shell elements were used to model the wing. Again, hard contact and frictionless impact conditions were applied to model the interaction between the tup and the composite wing. When analyzing the results of the FE simulation, it was found that the highest strain component is along the chord length so the FBG sensors were located and oriented as shown in Table 3.

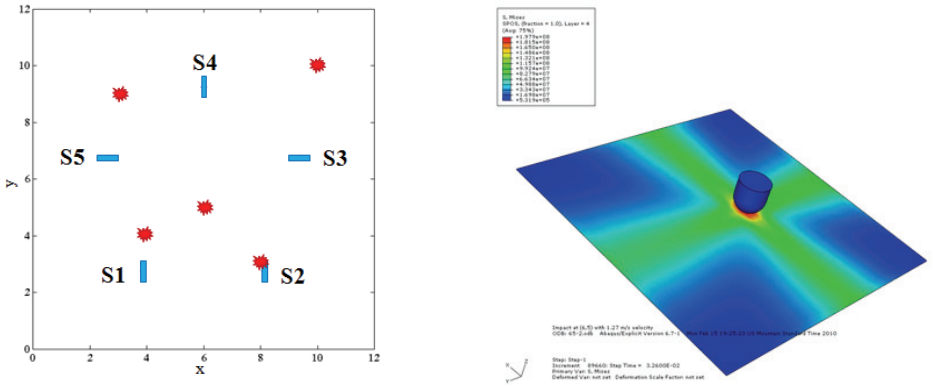

(a) (b)

Figure 2: (a) Locations of FBGs (blue) and impacts (red) [Plate dimensions in inches], (b) finite element simulation showing impact in composite plate

Table 3: Location of FBG sensors on composite wing structure.

Sensor Number	x-coordinate (in)	y-coordinate (in)	Measured strain component
S1	2	2	ε_{xx}
S2	11	2	ε_{xx}
S3	11	9	ε_{xx}
S4	2	9	ε_{xx}

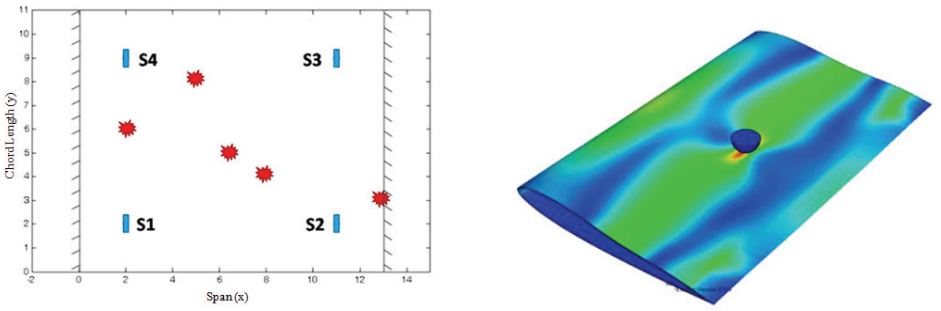

(a) (b)

Figure 3: (a) Schematic of wing showing boundary condition, location of FBGs (blue) and impacts (red) [Plate dimensions in inches], (b) finite element simulation showing impact on a composite wing.

5 Results and Discussion

5.1 Simulation Results

The data collected from the plate and wing simulations were smoothed to remove some minor perturbations in the sensor response in order to make algorithm training easier. Since the signal due to the impact is much larger than the noise present in the signal, smoothing does not adversely affect the result. To train the algorithm, strain data from four impact locations at all three energies were used to train the SVR algorithm and testing is done on the remaining unseen 50J impact. Figure 4 shows a sample load history prediction for impact at (8,4). It can be seen that the predicted loading is very similar to the simulated loading. In order to compare the time series from the simulation and the SVR algorithm, $\sigma_{\max}$ and area under the curve (AUC) were used. In the case of impact on a plate, the response looks Gaussian so it is possible to quantify the result in terms of the maximum value and the variance. However, for more complex structures, the response may not be Gaussian so AUC is a better metric for evaluating the result.

The results of the regression framework on a composite plate are shown in Table 4. It can be seen that the errors in the prediction of σ_{max} and AUC are less than 13 percent in all cases. It must be noted that since the simulated FBGs only measure strain in one direction, the strain information used to train the SVR algorithm is incomplete. In a complex structure where the measured loads behave more non-linearly with variation in impact location and energy, the prediction accuracy of this approach may be adversely affected. In order to mitigate this effect, a larger training set may be used.

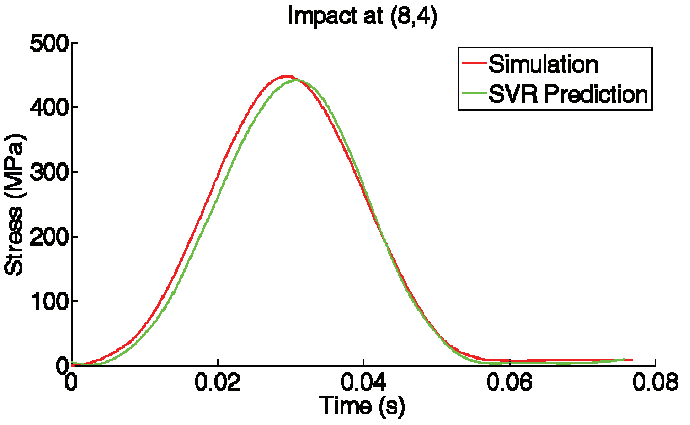

Figure 4: Simulated and predicted load history for impact at (8,4)

Table 4: Impact load history estimation result on composite plate

Impact location	Simulated σ_{max} (MPa)	Predicted σ_{max} (MPa)	Error	Simulated AUC (x10^6)	Predicted AUC (x10^6)	Error
(10,10)	895	882	1.45%	22.8	21.6	5.26%
(3,9)	988	882	10.73%	27.5	26.0	5.45%
(4,4)	753	848	12.62%	24.3	21.4	11.93%
(6,5)	780	750	3.85%	27.1	27.2	0.37%
(8,4)	821	842	2.56%	26.6	28.7	7.89%

For impact on a composite wing, strain data collected only in the direction of the chord length was used since the strains along the span were insensitive to some impacts. Since the changes in measured strain along the chord were larger than spanwise strain changes due to varying impact positions, it would provide better prediction results. During data analysis, it was found that only sensors 3 and 4 (Figure 3(a)) contributed useful information about the impact. During the impact, the trailing edge carries only small strains and as such, the information provided by sensors in this region may not be useful. This highlights the need for careful placement of the sensors on the wing so that all the sensors are able to provide useful data. For the current set of experiments, it was found that removal of information from sensor 1 and 2 did not change the result significantly so they were ignored in the interest of computational efficiency. The SVR framework has been trained using strains from all three impact energies at four locations with the test set being the fifth unseen 50J impact. Figure 5 shows the prediction result for an impact at

(5,8). It can be seen that while the algorithm is able to capture the general trend of the loading, the predicted shape differs from the simulated load.

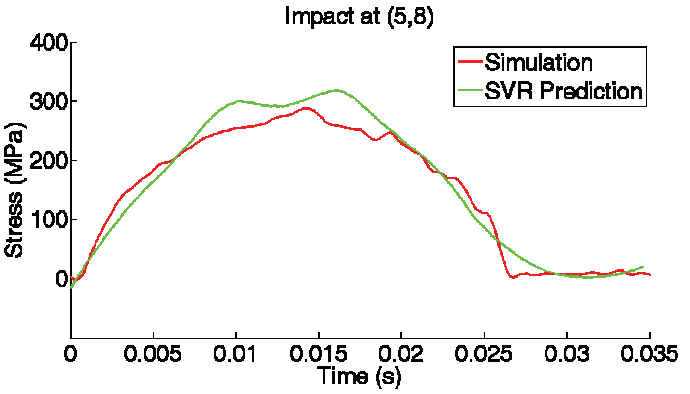

Figure 5: Simulated and SVR prediction result for impact at (5,8)

Table 5 shows the results of the load history reconstruction scheme when tested on a composite wing. For all impacts between sensor 3 and 4, the algorithm was able to estimate the load history to within 10% of σ_{max} and the AUC. For any point along the chord length, prediction results for impacts not between sensor 3 and 4 are inaccurate. One possible explanation for this might be a significant change in sensor response as the impact moves closer to the simply supported boundary condition. Inclusion of more training data closer to the simply supported region may improve the performance of the regression framework and will be investigated further in future work.

Table 5: Impact load history estimation on a composite wing

Impact location	Simulated σ_{max} (MPa)	Predicted σ_{max} (MPa)	Error	Simulated AUC (x10^6)	Predicted AUC (x10^6)	Error
(8,4)	531	514	3.20%	9.01	8.32	7.66%
(13,3)	577	479	16.98%	6.56	6.05	7.77%
(6.5,5)	541	522	3.51%	10.32	9.49	8.04%
(2,6)	639	522	18.31%	11.77	9.31	20.90%
(5,8)	576	636	10.42%	10.52	11.13	5.80%

5.2 Experimental Results

Experimental validation of the SVR impact estimation approach was conducted. The target variable used for prediction was the load measured by a dynamic load transducer at the tup and the input variables were the strains obtained using the output of the four FBG sensors. Figure 6 shows an example prediction for impact at (6.5,5). Although the amount of training data is limited, the algorithm is still able to capture the general trend of the loading during impact.

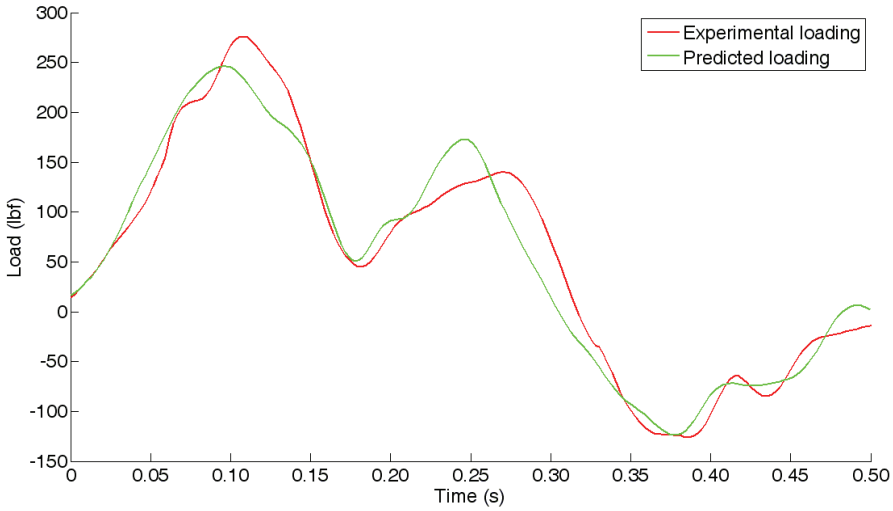

Figure 6: Experimental load cell reading and SVR prediction for impact at (6.5,5).

Table 6 shows the results of the SVR algorithm on the experimental data with the impact locations plotted in Figure 7. For impacts along the span, the algorithm was able to predict the load with accuracies greater than 90%. For impact sites along the chord length, the errors are much larger since there is a significant change in the sensor response due to varying curvature. It must also be noted that after the impact at (6.5,8) the wing started showing signs of matrix cracking and fiber breakage which became very large after the impact at (6.5,9) as shown in Figure 8. This accounts for the high prediction errors at these locations. The use of a larger training set along the chord length or knowledge of the complete strain state at every sensor location should improve prediction results along the chord length.

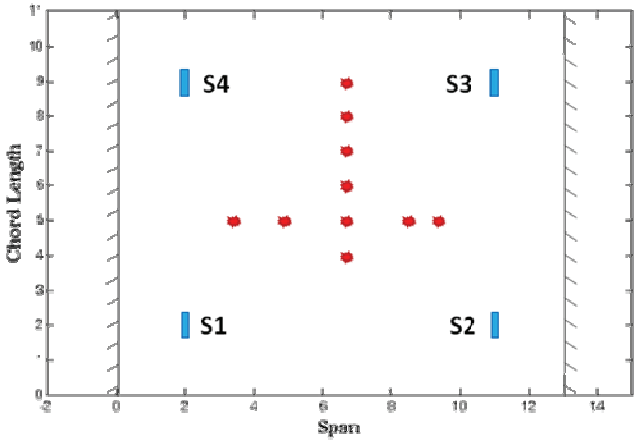

Figure 7: Locations of experimental impacts on the wing.

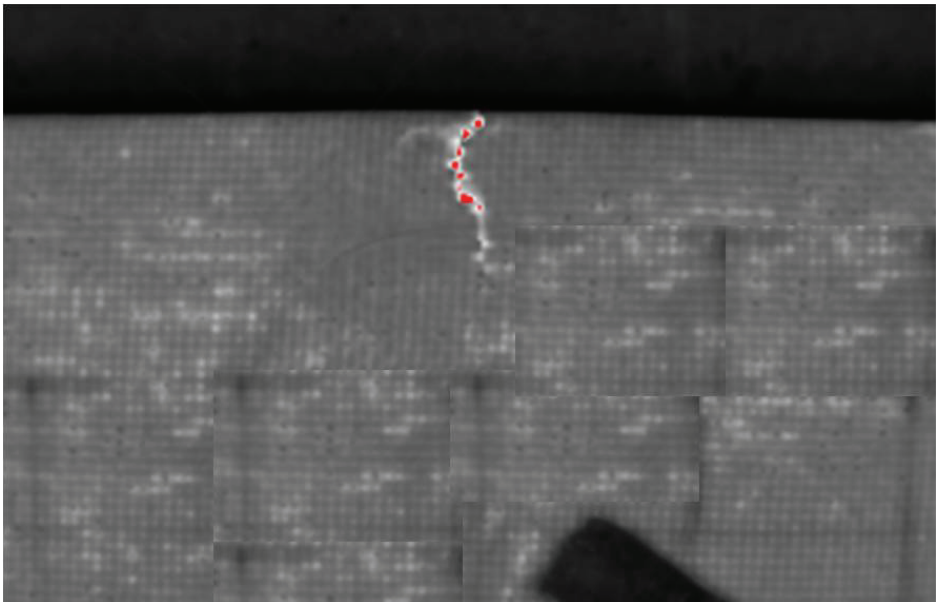

Figure 8: Thermographic image showing damage induced (red) on the leading edge of the composite wing after repeated impacts.

6 Concluding Remarks

A feature extraction and regression process was presented in this paper which allows for estimation of the impact load history in composite structures with complex

Table 6: Experimental prediction results for impact on a composite wing

Impact location	Expt Max Load (lbf)	Predicted Load (lbf)	Prediction Error	Expt AUC (lbf-s)	Predicted AUC (lbf-s)	Prediction Error
(3.5,5)	201.04	208.59	3.76%	2.49	2.62	5.22%
(5,5)	192.19	208.09	8.27%	2.58	2.60	0.78%
(6.5,5)	192.88	208.63	8.17%	2.54	2.61	2.76%
(8,5)	188.59	199.21	5.63%	2.47	2.55	3.24%
(9.5,5)	211.73	209.16	1.21%	2.74	2.63	4.01%
(6.5,4)	204.26	271.69	33.01%	2.49	2.98	19.68%
(6.5,5)	276.16	247.17	10.50%	2.83	2.75	2.83%
(6.5,6)	288.14	242.83	15.72%	3.05	2.60	14.75%
(6.5,7)	255.88	272.44	6.47%	2.85	2.68	5.96%
(6.5,8)	296.67	244.30	17.65%	3.47	2.60	25.07%
(6.5,9)	175.41	271.85	54.98%	2.32	2.91	25.43%

geometries. The framework developed uses time delay embedding to extract features that capture the dynamics of the system through FBG sensor response. Since the FBGs measure strain only in one direction, the strain information used for prediction is incomplete but still provides reasonable prediction results. Using an SVR algorithm, impact loads were predicted to within 12% on a composite plate and to within 10% on a composite wing when the impact was within the sensor network region. Inclusion of more simulation data in the training set is needed to improve the performance of the regression scheme. Experimental validation showed promising results even with small training sets. Since the change in measured strains is highly nonlinear along the chord length, more training impacts in that direction would help improve the performance of the estimator.

Acknowledgement: This research was supported by the NASA IVHM program; grant number NNX07AD70A, program manager Dr. Steven Arnold. The authors would also like to acknowledge Dr. Mark Seaver from the Naval Research Laboratory for his guidance during this project.

References

Aymerich and Meili (2000): Ultrasonic evaluation of matrix damage in impacted composite laminates. *Composites Part B: Engineering,* vol.31, no.1, pp.1-6.

Bednarcyk and M. (2002): *MAC/GMC 4.0 User's Manual. NASA/TM 2002-212077.*

Betz, Thursby, Culshaw and Staszewski (2007): Structural Damage Location with Fiber Bragg Grating Rosettes and Lamb Waves. *Structural Health Monitoring,* vol.6, no.4, pp.299-308.

Chan, Li and Ko (2001): Fatigue analysis and life prediction of bridges with structural health monitoring data – Part II: application. *International Journal of Fatigue,* vol.23, no.1, pp.55-64.

Coelho, Das and Chattopadhyay (2009): A Hierarchical Classification Scheme for Computationally Efficient Damage Classification. *Proc. IMechE, Part G: J. Aerospace Engineering,* vol.223, no.G5, pp.497-505.

Coelho, Das, Chattopadhyay, Papandreou-Suppappola and Peralta (2007): Detection of fatigue cracks and torque loss in bolted joints. *Health Monitoring of Structural and Biological Systems 2007,* vol.6532, pp.653204-653212.

Genest, Martinez, Mrad, Renaud and Fahr (2008): Pulsed thermography for non-destructive evaluation and damage growth monitoring of bonded repairs. *Composite Structures,* pp.(In Press).

Grondel, Assaad, Delebarre and Moulin (2004): Health monitoring of a composite wingbox structure. *Ultrasonics,* vol.42, no.1-9, pp.819-824.

Hiche, Liu, Seaver, Wei and Chattopadhyay (2009): Characterization of impact damage in woven fiber composites using fiber Bragg grating sensing and NDE. *Nondestructive Characterization for Composite Materials, Aerospace Engineering, Civil Infrastructure, and Homeland Security 2009,* vol.7294, pp.72940E-72911.

Huang, Chen, Hsu, Chen and Wu (2004): Credit rating analysis with support vector machines and neural networks: a market comparative study. *Decision Support Systems,* vol.37, no.4, pp.543-558.

Kim and Lee (2008): Identification of impact force in thick plates based on the elastodynamics and time-frequency method (II). *Journal of Mechanical Science and Technology,* vol.22, no.7, pp.1359-1373.

Kundu, Das, Martin and Jata (2008): Locating point of impact in anisotropic fiber reinforced composite plates. *Ultrasonics,* vol.48, no.3, pp.193-201.

Lee (2008): Identification of impact force in thick plates based on the elastodynamics and time-frequency method (I). *Journal of Mechanical Science and Technology,* vol.22, no.7, pp.1349-1358.

Lu, Lee and Chiu (2009): Financial time series forecasting using independent component analysis and support vector regression. *Decision Support Systems,* vol.47, no.2, pp.115-125.

Park and Chang (2005): System identification method for monitoring impact events. *Smart Structures and Materials 2005: Smart Sensor Technology and Mea-*

surement Systems, vol.5758, pp.189-200.

Shin, Lee and Kim (2005): An application of support vector machines in bankruptcy prediction model. *Expert Systems with Applications,* vol.28, no.1, pp.127-135.

Şimşir and Ankara (2007): Comparison of two non-destructive inspection techniques on the basis of sensitivity and reliability. *Materials & Design,* vol.28, no.5, pp.1433-1439.

Smola (1996): Regression estimation with support vector learning machines. Master's thesis,

Takens (1980): *Lecture Notes in Mathematics.* Springer.

Vapnik and Sterin (1977): On structural risk minimization or overall risk in a problem of pattern recognition. *Automation and Remote Control,*

Yu, Choi, Kweon and Kim (2006): A study on the failure detection of composite materials using an acoustic emission. *Composite Structures,* vol.75, pp.163–169.